Prognostic value of nuclear morphometry in myxoid liposarcoma

川口, 健悟

Received: 7 November 2022 | Revised: 20 December 2022 | Accepted: 16 January 2023

DOI: 10.1111/cas.15729

Cancer Science WILEY

ORIGINAL ARTICLE

Prognostic value of nuclear morphometry in myxoid liposarcoma

Kengo Kawaguchi[1,2] | Kenichi Kohashi[1] | Takeshi Iwasaki[1] | Takeo Yamamoto[1] | Shin Ishihara[1,2] | Yu Toda[1] | Hidetaka Yamamoto[1] | Yasuharu Nakashima[2] | Yoshinao Oda[1]

[1]Department of Anatomic Pathology, Graduate School of Medical Sciences, Kyushu University, Fukuoka, Japan

[2]Department of Orthopaedic Surgery, Graduate School of Medical Sciences, Kyushu University, Fukuoka, Japan

Correspondence
Yoshinao Oda, Department of Anatomic Pathology, Graduate School of Medical Sciences, Kyushu University, 3-1-1, Maidashi, Higashi-ku, Fukuoka, Japan.
Email: oda.yoshinao.389@m.kyushu-u.ac.jp

Funding information
Japan Society for the Promotion of Science, Grant/Award Number: 19H03444, 21K06887 and 21K20805

Abstract

Myxoid liposarcoma (MLS) accounts for 20%-30% of liposarcoma and the round cell component (RCC) is believed to be a specific poor prognostic factor. However, the RCC assessment criteria are vaguely defined and, therefore, are inconsistently employed by pathologists. In this study, we modified and applied two established grading systems to evaluate nuclear atypia (namely, the World Health Organization/International Society of Urological Pathology and the Fuhrman grading in renal cell carcinoma) in 64 MLS cases. Detailed software-based assessments of the morphology and the cellularity were performed. DNA mutation analysis, comprehensive mRNA expression analysis, and immunohistochemistry were also performed. Our findings revealed that the high–nuclear-grade group according to the modified Fuhrman grading system exhibited a significantly poor disease-free survival (hazard ratio: 4.43; 95% confidence interval: 0.9-22.6; $p = 0.047$). On the other hand, the cellularity was significantly higher in the modified Fuhrman high-grade group ($p = 0.010$ at the percentage of the hypercellular area; $p = 0.003$ at the maximum cell density) but did not qualify per se as a poor prognostic factor in the survival analyses. Furthermore, the modified Fuhrman high-grade group significantly expressed the cell cycle–related genes (such as *FOXM1*, *PLK1*, and *CDK1*). In conclusion, our analyses suggest that an evaluation focusing on nuclear morphology (rather than on cellular density) can be more reliable in predicting the MLS prognosis.

KEYWORDS
cell cycle–related gene, morphometry, myxoid liposarcoma, nuclear atypia, round cell component

Abbreviations: *CDK1*, cyclin-dependent kinase 1; CI, confidence interval; *DDIT3*, DNA damage–inducible transcript 3; DEG, differentially expressed gene; DFS, disease-free survival; FC, fold change; FFPE, formalin-fixed paraffin-embedded; FISH, fluorescence in situ hybridization; FNCLCC grade, French Fédération Nationale des Centers de Lutte Contre le Cancer grade; *FOXM1*, forkhead box protein M1; GO, Gene Ontology; HE, hematoxyrin and eosin; HPF, high-power field; HR, hazard ratio; MLS, myxoid liposarcoma; NGS, next-generation sequencing; OS, overall survival; *PLK1*, polo-like kinase 1; PPI, protein-protein interaction; p*TERT*, *TERT* promoter; RCC, round cell component; ROC, receiver-operating characteristic; RT-PCR, reverse-transcription polymerase chain reaction; *TERT*, telomerase reverse transcriptase; WHO/ISUP, World Health Organization/International Society of Urological Pathology.

1 | INTRODUCTION

Generally, malignant tumor cells have larger nuclei, irregular nuclear shape, and more distinct nucleoli than benign cells. These characteristics are often used to distinguish between benign and malignant tumors and to predict prognosis in many malignancies.[1–4]

Myxoid liposarcoma (MLS) accounts for 20%-30% of liposarcoma and is characterized by a DNA damage–inducible transcript 3 gene (*DDIT3*) rearrangement.[5] MLS exhibits two characteristically distinct cellular morphologies: conventional tumor cells with milder nuclear atypia and "classical" round cell components (RCC) with more severe nuclear atypias.[5,6] MLS cases with a certain percentage area of "classical" RCC have a poor prognosis.[5–13] However, a recent report examining only cases that were diagnosed strictly on genetic background, revealed that a "classical" RCC percentage area that is ≥5% cannot be associated with prognosis.[14] As far as the cutoff percentage of the "classical" RCC area is concerned, most studies assume it to be 5%; an assumption that is not consistently adopted, as both 5% and 25% cutoffs have been previously employed.[6,8–13,15,16] The use of a single cutoff value for all cases (irrespectively of the tumor size) has been cited as a problem, as it does not reflect the absolute amount of the malignant components.[6] Moreover, no clear definition of the "classical" RCC exists: "Classical" RCC has been regarded as the area composed of "round" cells in hypercellularity with a nuclear overlap, while a clear definition of the RCC is occasionally abbreviated in studies.

The aim of this study was to investigate the nuclear morphology, cell density, and genetic background of MLS cases corroborated through the detection of fusion genes. In addition, we explored evaluation methods that could be more reliable in predicting MLS prognosis.

2 | MATERIALS AND METHODS

2.1 | Patients and tumor selection

A total of 64 primary MLS cases were included in the present study from the archive of the Department of Anatomic Pathology of Kyushu University (Fukuoka, Japan) between 1976 and 2021. These patients underwent surgical resection without receiving any preoperative treatment. Apart from these 64 cases included in the survival analysis, four cases of primary and metastatic recurrence (a total of nine specimens) as well as two specimens from relapsing lesions that had undergone preoperative treatment were also used for DNA target sequencing. In addition, clinical information was retrospectively obtained from the medical records. The depth of the tumor's location was classified by considering the fascia as the border. The present study was conducted under the principles embodied in the Declaration of Helsinki and was approved by the institutional review board (IRB) of Kyushu University (IRB number 29-429 and 29-625).

2.2 | Histological review

All hematoxyrin and eosin (HE)-stained slide specimens were reviewed and evaluated by two pathologists on the following factors: the French Fédération Nationale des Centers de Lutte Contre le Cancer (FNCLCC)-grade[5] cellularity, and the percentage of "classical" RCC. The FNCLCC grade was scored by the following factors: tumor differentiation (MLS: score 2; high-grade MLS: score 3), mitotic activity (0-9; 10-19; ≥20 at 10 high-power fields [HPFs]), and tumor necrosis (absent; <50%; ≥50%). The "classical" RCC was defined as the area composed of "round"-shaped tumor cells with nuclear overlap at a glance. The cases with ≥5% of "classical" RCC were assigned tumor differentiation score 3 in FNCLCC grading. The hypercellular area was defined as that with a nuclear overlap, regardless of the nuclear morphology. Pathologists evaluated the percentage of the hypercellular area in the whole of the obtained slides in each case.

2.3 | Modified Fuhrman and WHO/ISUP grading

We evaluated the nuclear morphology by using the modified Fuhrman and World Health Organization/International Society of Urological Pathology (WHO/ISUP) grading systems (Figure 1). The original Fuhrman and WHO/ISUP grading systems represent methods that assess the nuclear morphology in renal cell carcinoma to predict prognosis.[4,17,18] The present study used the modified versions as shown in Table 1. The highest grade in the specimen was adopted in either grading system, as in the original ones. We assessed the reliability of both grading systems by employing weighted Cohen's kappa coefficients, calculated for the grades independently assessed by two pathologists.[19,20]

2.4 | Evaluation of cellularity and nuclear morphology using software

We used two software packages to evaluate cellularity and nuclear morphology: Hybrid Cell Count (BZ-X800, Keyence)[21] and QuPath (version 0.3.2; an open-source software for digital pathology images).[22] For the Hybrid Cell Count, we took three HPFs per case carrying the greatest cell density at a glance, and semiautomatically analyzed them for the density and morphological parameters as follows: nuclear area, roundness, and circularity calculated, respectively, by the following equations: $\text{Roundness} = \frac{\text{Diametermax.} - \text{Diameter min.}}{2}$; $\text{Circularity} = \frac{4\pi \times \text{Area}}{\text{Perimeter}^2}$. Roundness indicates rough morphology of the nucleus. Circularity, on the other hand, is defined by area and perimeter and is influenced more by the perimeter, which reflects the degree of irregularity of the nuclear rim. For the QuPath, we selected 10 cells per case with the most prominent nucleus in HPFs, and we manually traced the nucleus' margins. The morphological parameters above were analyzed, and the mean values were adopted.

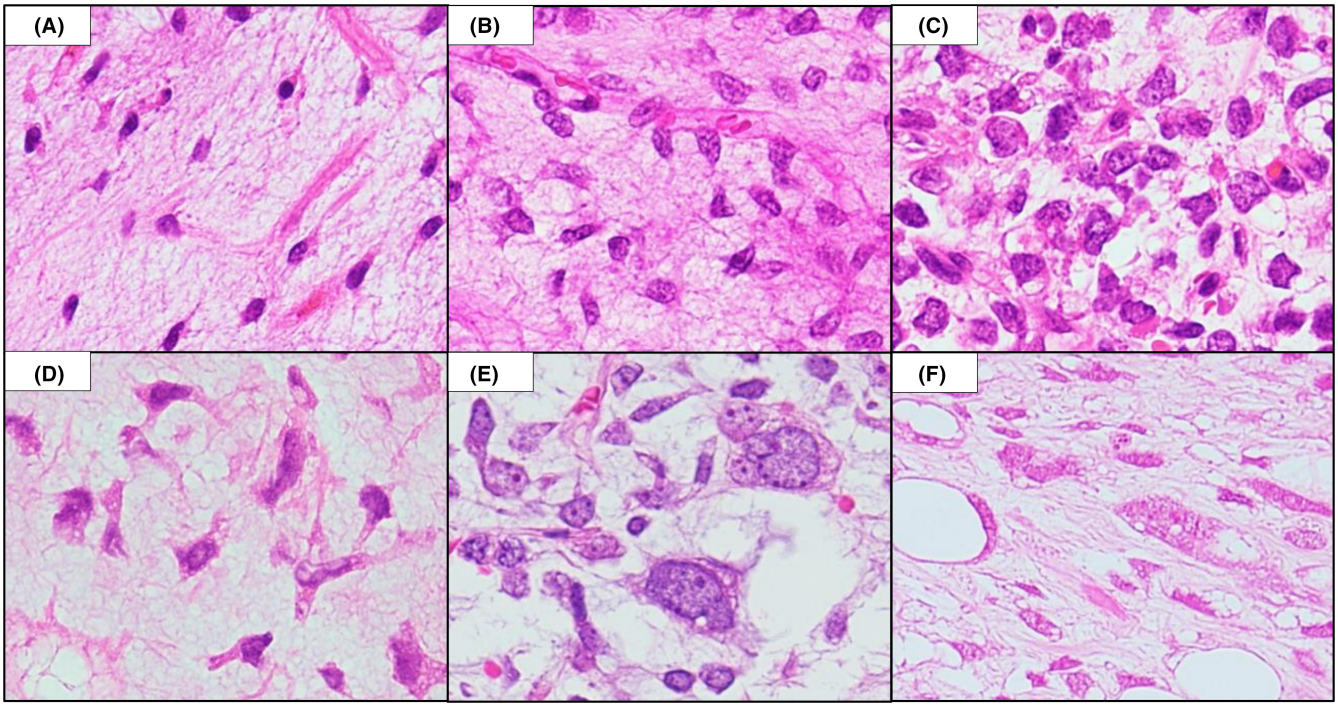

FIGURE 1 Histology of myxoid liposarcoma (MLS), as assessed by the modified Fuhrman grading system in high-power fields (HE; ×400). Grade 1 with small nuclei and no visible nucleoli (A). Grade 2 with slightly larger nuclei and visible nucleoli only in the high-power field (HPF) (B). Grade 3 with larger nuclei and distinct nucleoli (C). Grade 2 in the modified World Health Organization/International Society of Urological Pathology (WHO/ISUP) grading due to the hyperchromatic nuclei and no visible nucleoli in the ×100 magnification, but with larger and irregular-shaped nuclei suggesting a modified Fuhrman grade 3 (D). Grade 4 with anaplastic tumor cells having significantly larger or extremely irregular-shaped nuclei (E, F). The features are not assigned to "classical" RCC due to the lower cell density, although they qualify as high grade based on the modified Fuhrman and WHO/ISUP grading systems (C-F)

TABLE 1 Outlines of modified World Health Organization/International Society of Urological Pathology (WHO/ISUP) grade and modified Fuhrman grade

Grading system	Grade 1	Grade 2	Grade 3	Grade 4
Modified WHO/ISUP	Absent or basophilic, inconspicuous nucleoli at ×400 magnification	Nucleoli conspicuous and eosinophilic at ×400 magnification and visible but not prominent at ×100 magnification	Nucleoli conspicuous and eosinophilic at ×100 magnification	Tumor giant cells and extreme nuclear pleomorphism with clumping of chromatin
Modified Fuhrman	Small (the same size as lymphocytes) uniform nuclei with absent or inconspicuous nucleoli	Larger (1-2 lymphocytes) nuclei with irregularities in outline and with nucleoli visible at ×400 magnification	Even larger nuclei (>2-3 lymphocytes) with an obvious irregular outline and nucleoli visible at ×100 magnification	Large and pleomorphic cells and heavy chromatin clumps, extreme irregularoutlines

These grading systems were modified from the original Fuhrman grading[18] and WHO/ISUP grading.[17]
The largest grade among the evaluated sections is adopted for the case.

2.5 | DNA extraction

Genomic DNA was extracted from fresh-frozen specimens and formalin-fixed paraffin-embedded (FFPE) specimens. We followed the manufacturer's protocols for all procedures, as previously described.[23] In the FFPE specimens, each of the two regions (high and low nuclear grade) was collected by scraping under visual inspection (Figure S1A and Table S1).

2.6 | RNA extraction

According to the manufacturer's protocol, the total RNA was extracted from only the FFPE specimens by using RNAstorm™ FFPE RNA Extraction Kit (Cell Data Science). The samples were collected from two regions (high and low nuclear grade) in the same manner as the DNA extraction (Figure S1A and Table S2).

2.7 | Detection of gene rearrangement

All eligible cases were subjected to fluorescence in situ hybridization (FISH) or reverse transcription (RT)-PCR, followed by direct sequencing to confirm the *DDIT3* rearrangement. We used the Vysis DDIT3 Break Apart FISH Probe kit (Abbott Laboratories) for FISH. The methods and the primers' settings for the RT-PCR and direct sequencing were the same as previously reported.[24]

2.8 | Next-generation sequencing (NGS) for targeted genes

Formalin-fixed paraffin-embedded samples were available in six regions of three cases (two regions of different nuclear grades in each case: cases 1-3), and 18 frozen samples were also available (cases 4-14) (Table S1). As previously reported, we performed NGS for targeted genes and followed the manufacturer's protocols for all subsequent experimental procedures.[23] The details are noted in Doc S1.

2.9 | Direct sequencing for telomerase reverse transcriptase (*TERT*) promoter hot spots

Reverse-transcription PCR and direct sequencing were performed to detect gene mutations in the *TERT* promoter (p*TERT*) hot spots for the same DNA samples used in the NGS mentioned above. The methods and the primers' design were as previously described.[23]

2.10 | mRNA expression and bioinformatics analysis

We assessed the comprehensive mRNA expression by using the nCounter® Gene Expression Assay (NanoString Technologies Inc.). All 12 samples were extracted from FFPE, and had tumor cells of each nuclear grade confirmed histologically. The details of the specimens are shown in Table S2. The extracted mRNA samples were enriched for target regions for the nCounter® Human Tumor Signaling 360™ Panel (https://nanostring.com/products/ncounter-assays-panels/oncology/tumor-signaling-360/) and were measured using the nCounter® Analysis System (NanoString Technologies Inc.). Finally, the raw data were normalized using nSolver™ Analysis Software (version 4.0, NanoString Technologies Inc.). We followed the manufacturer's protocols for all the procedures mentioned above.

Differentially expressed genes (DEGs) with a $|\log_2(\text{FC [fold change]})|$ that was >1 and a *P* value that was <0.05 between the nuclear high-grade and low-grade groups were identified using the edgeR package in R.[25] DEGs were evaluated by the value of the high–nuclear-grade group relative to the low-grade group. To exclude the influence of case-specific or cellularity-induced gene profiles among the DEG candidates obtained in cases 15-20, only those genes that demonstrated the same trend in each of cases 1-3 were retrieved as true DEGs for the following analyses.

We acquired an overview of the DEGs using the Database for Annotation, Visualization, and Integrated Discovery that is available online for Gene Ontology (GO) analysis,[26] as well as using the ReactomePA package in R for Reactome pathway analysis.[27] Moreover, to identify the hub genes, we developed a protein-protein interaction (PPI) network using stringApp; an application on Cytoscape (version 3.9.1).[28] Subsequently, we performed a topological analysis on the network using NetworkAnalyzer, a Cytoscape application.[29] The degree centrality was calculated. Finally, the top 20 genes, characterized by the most significant degree centrality, were identified as hub gene candidates.

2.11 | Immunohistochemistry

The surgically resected sections of the highest nuclear grade were selected in each case, and FFPE specimens were prepared for immunohistochemical study. We used primary antibodies against the forkhead box protein M1 (FOXM1; 1:100; rabbit monoclonal, ab207298; Abcam), polo-like kinase 1 (PLK1; 1:100; rabbit monoclonal, 4513; Cell Signaling Technology), and cyclin-dependent kinase 1 (CDK1; 1:100; mouse monoclonal, MA5-11472; Thermo Fisher Scientific).

Immunohistochemical staining was independently assessed by two pathologists. The nuclear staining intensity was classified into four categories: "0" for negative staining, "1" for weak staining, "2" for moderate staining, and "3" for strong staining. For FOXM1 and PLK1, we regarded tumor cells with a nuclear staining intensity ≥2 as positive and evaluated the labeling index in a hot spot (Figure S1B). A labeling index ≥3% was defined as indicative of a positive case for FOXM1, and the existence of any positive tumor cells was defined as a positive case for PLK1. On the other hand, for CDK1, the H-score was calculated as previously described (Figure S1B).[30,31] An H-score ≥75 was defined as indicative of a positive case for CDK1. These cut-off values were determined by a time-dependent receiver-operating characteristic (ROC) curve, as described below.

2.12 | Statistical analysis

All statistical analyses were conducted using R (version 4.1.2; R Foundation for Statistical Computing). Statistical significance was defined when a *P* value was found to be <0.05. Overall survival (OS) was defined as the duration between the date of the tumor resection and death, while disease-free survival (DFS) was defined as the duration from the date of the tumor resection to identification of a distant metastasis or local recurrence. Survival curves for OS and DFS were estimated by using the Kaplan-Meier method and were compared statistically by using the log-rank test. Moreover, using the Cox univariate regression models, the hazard ratio (HR) and the 95% confidence interval (95% CI) were estimated. Fisher's exact tests and Mann-Whitney *U* tests were performed to compare categorical and

quantitative variables between the two corresponding groups. For factors with no established cutoff values available, the cutoff values were decided by the time-dependent ROC curve at 5 years DFS, and were adopted to facilitate clinical application.[32]

3 | RESULTS

3.1 | Clinicopathological characteristics

Clinical and pathological findings are summarized in Table 2. The 64 MLS cases corresponded to 34 males and 30 females with a median age of 48 years (interquartile range [IQR]: 38-59). Nine cases (14.1%) had ≥5% of "classical" RCC and were assigned a tumor differentiation score of 3 in the FNCLCC grading. On the other hand, 42 (65.6%) cases scored as G2 in the FNCLCC histological grading.

The survival curves of the Kaplan-Meier method are presented in Figure S2. The median follow-up was 49 months (IQR: 29-100). The higher FNCLCC histological grade (G2) was the only factor associated with a significantly poor DFS. A "classical" RCC ≥5% was not statistically associated with either the OS or DFS. However, the presence of a "classical" RCC exhibited a trend toward poor DFS, although it was not statistically significant ($p = 0.15$).

3.2 | Nuclear morphology evaluated by modified Fuhrman and WHO/ISUP grading

A breakdown of the cases with modified WHO/ISUP and Fuhrman grades is provided in Table 2. The cases with grade 4 were sporadic (2 in 64 cases). Grades 3 and 4 were regarded as high nuclear grade, whereas grades 1 and 2 we regarded as low nuclear grade. In total, 41% and 44% of the cases according to the modified WHO/ISUP and Fuhrman gradings, respectively, were assigned to the high–nuclear-grade groups. With regard to the survival analysis, high–nuclear-grade groups were characterized by a significantly poor DFS (HR: 5.17, 95% CI: 1.0-25.7, $p = 0.025$ by the modified WHO/ISUP grading; HR: 4.43, 95% CI: 0.9-22.6, $p = 0.047$ by the modified Fuhrman grading) as well as by trends of a poor OS without statistical significance (HR: 5.96, 95% CI: 0.7-53.8, $p = 0.071$ by the modified WHO/ISUP; HR: 5.44, 95% CI: 0.6-49.0, $p = 0.090$ by the modified Fuhrman grading) (Figure 2A). We describe below the modified Fuhrman grading mainly because there was no other significant statistical difference identified between the modified Fuhrman and WHO/ISUP grading systems with regard to the survival analysis, while the modified Fuhrman grading was a more embracing evaluation method that included the nuclear size in addition to those of the WHO/ISUP grading.

In the relevance between the modified Fuhrman grading and the clinicopathological findings, the high–nuclear-grade group included more cases with a higher FNCLCC histological grade ($p < 0.001$), with necrosis ($p = 0.021$), and with "classical" RCC that was ≥5% ($p = 0.008$) (Table 3). However, a relatively large number of high–nuclear-grade cases were characterized by a "classical" RCC that was <5% (Table 3). Cohen's weighted kappa (as calculated by two

TABLE 2 Clinicopathological features

Factor	Group	*n* (%) 64
Sex	Male	34 (53.1)
	Female	30 (46.9)
Age (years)	<55	43 (67.2)
	≧55	21 (32.8)
Median age [IRQ]		47.50 [38.25, 59.25]
Location	Limb, proximal	55 (85.9)
	Limb, destal	6 (9.4)
	Trunk	2 (4.7)
Part	Deep	44 (77.2)
	Superficial	12 (21.1)
	Abdominal cavity	1 (1.8)
Size (cm)	<9	31 (48.4)
	≧9	28 (43.8)
	Unknown	5 (7.8)
Median size [IQR]		8.00 [6.00, 11.25]
Fusion gene	*FUS*	48 (75.0)
	EWSR1	3 (4.7)
	Unknown	13 (20.3)
"Classical" RCC (%)	<5	55 (85.9)
	≧5	9 (14.1)
FNCLCC histologic grade	1	22 (34.4)
	2	42 (65.6)
	3	0 (0)
Mitotic count	0-9	61 (95.3)
	10-19	3 (4.7)
	≧20	0 (0)
Necrosis	None	27 (42.2)
	<50	37 (57.8)
	≧50	0 (0)
Modified WHO/ISUP grade	1	16 (25.0)
	2	22 (34.4)
	3	24 (37.5)
	4	2 (3.1)
Modified Fuhrman grade	1	8 (12.5)
	2	28 (43.8)
	3	26 (40.6)
	4	2 (3.1)

Abbreviations: FNCLCC, Fédération Nationale des Centers de Lutte Contre le Cancer; IQR, interquartile range; RCC, round cell component; WHO/ISUP, World Health Organization/International Society of Urological Pathology.

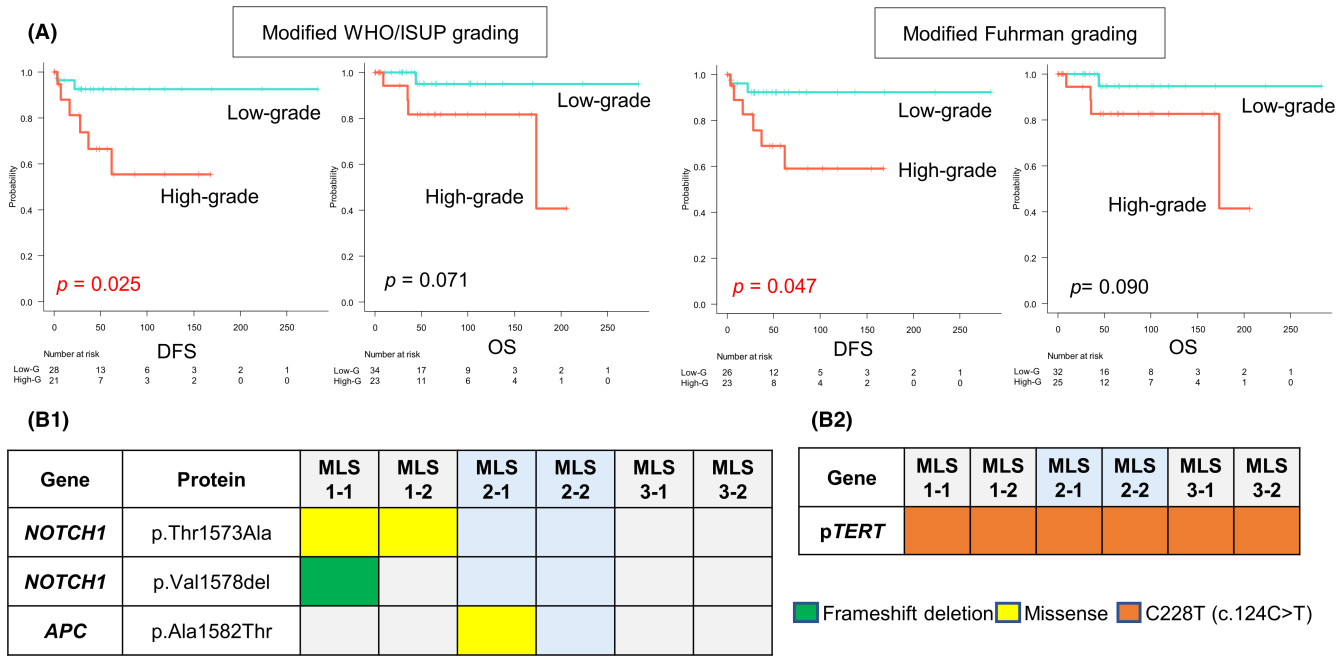

(B1)

Gene	Protein	MLS 1-1	MLS 1-2	MLS 2-1	MLS 2-2	MLS 3-1	MLS 3-2
NOTCH1	p.Thr1573Ala						
NOTCH1	p.Val1578del						
APC	p.Ala1582Thr						

(B2)

Gene	MLS 1-1	MLS 1-2	MLS 2-1	MLS 2-2	MLS 3-1	MLS 3-2
p*TERT*						

Frameshift deletion Missense C228T (c.124C>T)

FIGURE 2 Results of the survival analyses of the modified World Health Organization/International Society of Urological Pathology (WHO/ISUP) and Fuhrman gradings and of the mutation analyses. Grades 1 and 2 were defined as low-grade groups, and grades 3 and 4 were defined as high-grade groups in each of the herein examined grading systems. The high-grade groups exhibited a significantly poor disease-free survival (DFS) in both gradings. Moreover, the trends of poor overall survival (OS) in high-grade groups are noted (A). The mutations detected by next-generation sequencing (NGS) (B1) and direct sequencing (B2) in paired cases (MLS1-3). Only a few mutations were captured, and no consistent trends were identified between the low-grade (MLS1-1, 2-1, and 3-1) and the high-grade (MLS1-2, 2-2, and 3-2) samples (B1). All six samples in these three cases bear a p*TERT* hot spot mutation, C228T (c.124C>T), that is known as a major mutation (B2)

pathologists) was found to be 0.743 and 0.752 for the modified WHO/ISUP and Fuhrman gradings, respectively.

3.3 | Cellularity and nuclear morphological parameters

The group with any portion of the hypercellular area had trends of poor prognosis without statistical significance ($p = 0.15$ for DFS, and $p = 0.56$ for OS). For the maximum nuclear density per HPF of the device (1 HPF equals 0.08 mm^2, as calculated through the Hybrid Cell Count software), the cutoff was 360 nuclei/HPF. The group with ≥360 nuclei/HPF exhibited a trend of association with poor DFS ($p = 0.090$) but had no association with the OS ($p = 0.91$) in the survival analysis.

The relevance between the cellularity, the nuclear morphological parameters, and the modified Fuhrman grading is shown in Figure S3. The percentage of the hypercellular area and the nuclear density were significantly larger in the high–nuclear-grade group than in the low–nuclear-grade group ($p = 0.010$ and $p = 0.003$, respectively). In addition, the high–nuclear-grade group had a larger nuclear area in both measurement methods ($p < 0.001$ in QuPath and $p = 0.018$ in Hybrid Cell Count). Roundness did not differ by the nuclear grade. On the other hand, circularity was significantly lower in the high–nuclear-grade group as measured by the Hybrid Cell Count ($p = 0.003$), suggesting that the high–nuclear-grade group might have more complex nuclear rims.

3.4 | DNA mutations by NGS

The somatic mutations detected by NGS are shown in Figure 2B1, but they were not consistent with each nuclear grade. Furthermore, no consistent mutations were detected between primary and relapsing cases or between good and poor prognosis cases (Figure S4A).

3.5 | *TERT* promoter hot spot mutations

Mutations in p*TERT* hot spots were detected in 17 out of 24 samples (70.8%): all detected mutations were C228T (c.-124C>T), the most commonly reported mutation (Figure 2B2).[14,33,34] As with the NGS mutation analysis, no consistent trend was identified for p*TERT* mutations between primary and relapsing cases or good and poor prognostic cases (Figure S4A).

3.6 | Comprehensive mRNA expression analysis

We performed a comprehensive mRNA expression analysis by using nCounter® and drawing heatmaps, as shown in Figure 3A. The cases were classified into two clusters of independent cases (cases 15-20; MLS 15-20) (Figure 3A1). The clusters were consistent with the

TABLE 3 Relevance between modified WHO/ISUP/modified Fuhrman grade and clinicopathological features

		Modified WHO/ISUP grade *n* (%)			Modified Fuhrman grade *n* (%)		
		1 and 2	3 and 4	*P* value	1 and 2	3 and 4	*P* value
Factor	**Group**	***n* = 38**	***n* = 26**		***n* = 36**	***n* = 28**	
Sex	Male	16 (42.1)	18 (69.2)	**0.043**	14 (38.9)	20 (71.4)	**0.012**
	Female	22 (57.9)	8 (30.8)		22 (61.1)	8 (28.6)	
Age (years)	<55	26 (68.4)	17 (65.4)	>0.99	25 (69.4)	18 (64.3)	0.79
	≧55	12 (31.6)	9 (34.6)		11 (30.6)	10 (35.7)	
Location	Limb, proximal	32 (84.2)	23 (88.5)	>0.99	30 (83.3)	25 (89.3)	0.69
	Limb, distal	4 (10.5)	2 (7.7)		4 (11.1)	2 (7.1)	
	Trunk	2 (5.3)	1 (3.8)		2 (5.6)	1 (3.6)	
Depth	Deep	27 (79.4)	17 (73.9)	0.52	25 (78.1)	19 (76.0)	0.75
	Shallow	6 (17.6)	6 (26.1)		6 (18.8)	6 (24.0)	
	Abdominal cavity	1 (2.9)	0 (0.0)		1 (3.1)	0 (0)	
Size (cm)	<9	19 (54.3)	12 (50.0)	0.80	19 (57.6)	12 (46.2)	0.44
	≧9	16 (45.7)	12 (50.0)		14 (42.4)	14 (53.8)	
Fusion gene	*FUS*	31 (81.6)	17 (65.4)	0.55	29 (80.6)	19 (67.9)	0.56
	EWSR1	1 (2.6)	2 (7.7)		1 (2.8)	2 (7.1)	
	Unknown	6 (15.8)	7 (26.9)		6 (16.7)	7 (25.0)	
"Classical" RCC (%)	<5	37 (97.4)	18 (69.2)	**0.002**	35 (97.2)	20 (71.4)	**0.008**
	≧5	1 (2.6)	8 (30.8)		1 (2.7)	8 (29.6)	
FNCLCC histological grade	1	19 (50.0)	3 (11.5)	**0.001**	20 (54.1)	2 (7.4)	**<0.001**
	2	19 (50.0)	23 (88.5)		17 (45.9)	25 (92.6)	
Mitotic count	0-9	38 (100.0)	23 (88.5)	0.062	36 (100.0)	25 (89.3)	0.079
	10-19	0 (0.0)	3 (11.5)		0 (0)	3 (10.7)	
Necrosis	None	20 (52.6)	7 (26.9)	0.070	20 (55.6)	7 (25.0)	**0.021**
	<50	18 (47.4)	19 (73.1)		16 (44.4)	21 (75.0)	

Abbreviations: FNCLCC, Fédération Nationale des Centers de Lutte Contre le Cancer; RCC, round cell component; WHO/ISUP, World Health Organization/International Society of Urological Pathology.

The bold values indicate with $p < 0.05$.

groups identified by the modified Fuhrman grading. Paired samples of three cases (cases 1-3; MLS 1-3) were also clustered almost independently by histological nuclear grades (Figure 3A2). In all of the undertaken sample analyses, the sample corresponding to the modified Fuhrman grade 4 (case 18; MLS 18) exhibited a unique gene expression pattern (Figure S4B).

We determined DEGs (55 upregulated and 20 downregulated genes) for the assessments presented in Table S3. In the GO and Reactome analyses, more upregulated genes were significantly detected in the cell cycle (Figure 3B,C). The results of the analyses for the downregulated DEGs are presented in Figure S4C,D.

In addition, we developed a PPI network allowing us to search for more influential DEGs to determine the target genes in the following analysis (Figure 3D). One larger cluster was detected, and we also identified 20 candidates for hub genes with a higher degree centrality in terms of topology analysis (Table S3). We retrieved three of these hub genes (namely, *FOXM1*, *PLK1*, and *CDK1*) after considering the degree of fold change, statistical significance, and the possibility of them being associated with MLS.

3.7 | Immunohistochemical validation and relevance with nuclear grade

For the three genes identified by the PPI network, the protein expression was examined through immunohistochemical staining of the FFPE specimens. The expression levels of each protein and the comparison between the modified Fuhrman high and low grades are shown in Figure S5A. The FOXM1, PLK1, and CDK1 proteins all expressed significantly higher positive rates in the high–nuclear-grade group ($p < 0.001$ in the cases of FOXM1 and CDK1, and $p = 0.001$ in the case of PLK1). In the survival analysis, the positive-expression groups exhibited trends toward poorer DFS in all proteins without statistical significance. The evaluations combined with the expression of each protein are presented in Figure S5B. The group that was positive for both FOXM1 and CDK1 was characterized by a significantly poorer DFS than other combinations (HR: 4.38, 95% CI: 1.0-19.8, $p = 0.033$), while the group with a combination of PLK1 and CDK1 positivity was characterized by a trend of association with poor DFS (HR: 3.54, 95% CI: 0.8-15.9, $p = 0.071$).

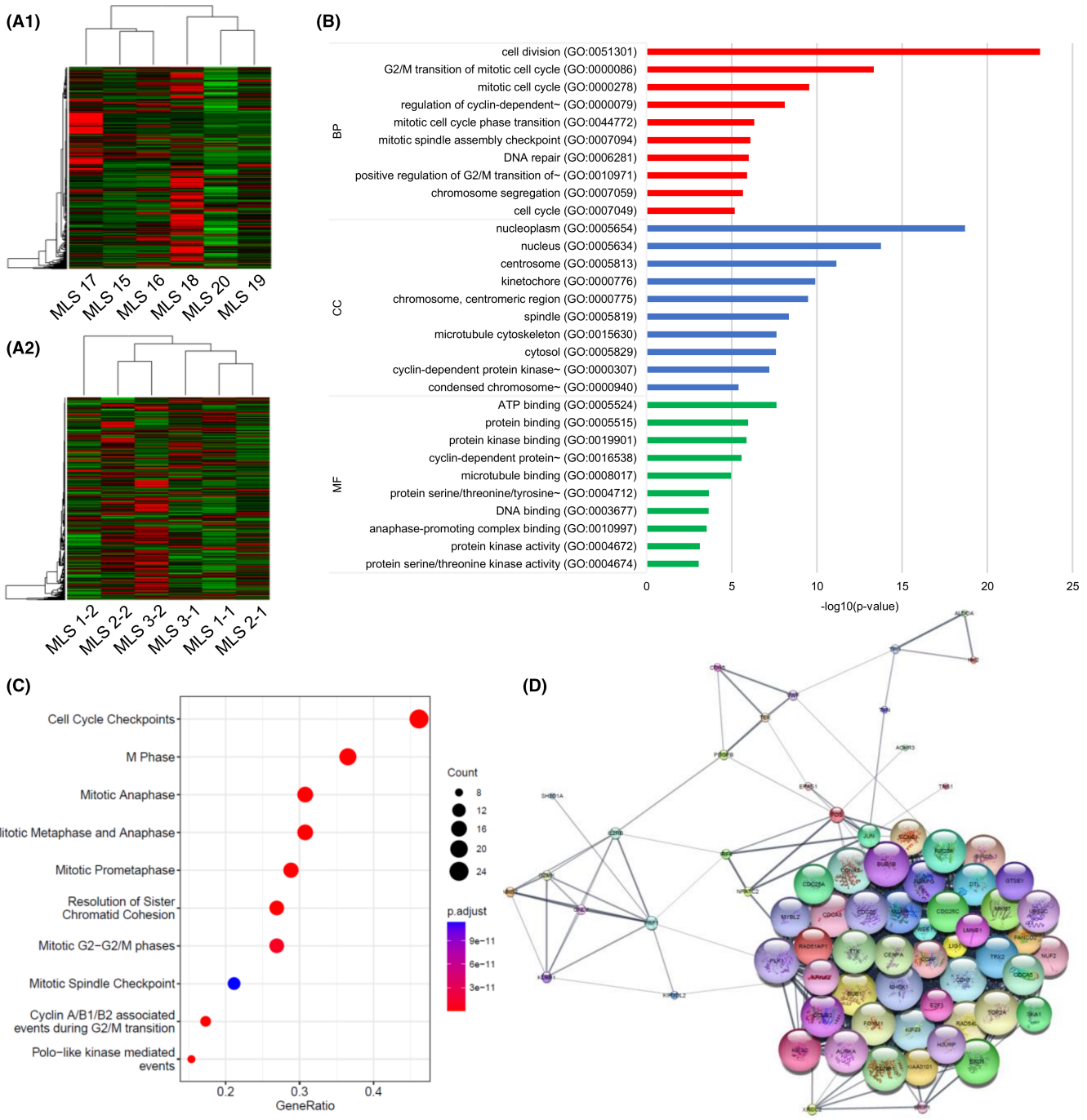

FIGURE 3 mRNA expression heatmaps, the Gene Ontology (GO) and Reactome pathway analyses, and the protein-protein interaction (PPI) network of the upregulated differentially expressed genes (DEGs). The clustering was similar to that of the histological nuclear grading among paired cases (cases 1-3) (A2). In addition, the drawn clusters were consistent with those of histological grouping among independent cases (cases 15-20) (A1). MLS1-1, 2-1, 3-1, 15, 16, and 17; modified Fuhrman low-grade. MLS1-2, 2-2, 3-2, 18, 19, and 20; modified Fuhrman high-grade. GO and Reactome analyses show that the cell cycle–related genes are significantly upregulated (B, C). The drawn PPI network with one large cluster (D). A topology analysis was performed on this network. The size of each node reflects the resulting degree of centrality (D)

4 | DISCUSSION

The present study investigated the nuclear morphology and cellularity in detail, and unveiled the genetic features of MLS cases corroborated by the identification of fusion genes. We also attempted to develop histological evaluation methods that were clearer, more reliable, and more helpful in predicting MLS prognosis. The high–nuclear-grade group (as evaluated by a modified WHO/ISUP and Fuhrman grading) exhibited a significantly poorer prognosis. Hypercellularity was significantly greater in the high–nuclear-grade

group of the modified Fuhrman grading, as assessed both by pathologists and a software. The clusters generated by gene expression heatmaps were mainly consistent with those identified by the modified Fuhrman grading. Furthermore, the expression of cell cycle–related genes was significantly higher in the high–nuclear-grade group than in the low–nuclear-grade group.

In the present study, the results from the survival analysis regarding the "classical" RCC differed from those of older reports[9,10,15] but were compatible with a relatively newer one.[14] Previous studies included more cases with an RCC ≥5% than the present study,[9–11,35] which can be due to the inconsistency regarding the definition of the RCC. The FNCLCC score was reaffirmed as a useful prognostic predictor; however, it may be inappropriate due to the fact that the differentiation score requires the evaluation of the "classical" RCC, which is an uncertain factor.

Cellularity revealed no association with prognosis, while nuclear atypia based on the modified WHO/ISUP and Fuhrmann grades was strongly related to MLS prognosis. Hence, nuclear morphology—rather than cell density—can be a more critical factor in predicting the MLS prognosis. As significant differences were detected in the survival analysis of a single factor, the nucleoli (modified WHO/ISUP grading) were assumed to be the most important prognostic predictor. However, further validation of the usefulness of the modified Fuhrman and WHO/ISUP grading by multivariable analysis in larger-scale studies are required. Future basic research is expected to elucidate the mechanisms by which the nucleoli and nuclear morphology (size and rim shape) contribute to malignancy. Cases with poor prognosis may have been underestimated, as more high–nuclear-grade cases in the modified Fuhrman grading did not meet the "classical" RCC ≥5% criterion. Furthermore, the modified WHO/ISUP and Fuhrman grades were decided based on the assessment of the highest-grade cells in each specimen. This finding implies that these two methods can be more efficient than the evaluation of the "classical" RCC, which cannot be determined without the use of a vast number of slides. Modified Fuhrman high-grade cases had greater cellularity than the low-grade group, suggesting that hypercellularity is a confounding factor for abnormal nuclear morphology. With respect to the morphological parameters, the roundness did not differ by nuclear grade, suggesting that tumor cells with larger nuclei have been classically recognized as typical "round cells." The larger nucleus may make the cell appear round in general. Alternatively, the circularity calculated by the Hybrid Cell Count software revealed more complex nuclear rims in the high–nuclear-grade group. Hence, the broad understanding of high–nuclear-grade tumor cells as "round" cells in MLS might not accurately reflect the feature, and a description of tumor cells as having "larger" or "more complex-shaped" nuclei may be more appropriate. Based on the result of the weighted Cohen's kappa coefficients, the inter-rater reliabilities of these grading systems were substantial, and they can be used in clinical situations.

Next-generation sequencing and direct sequencing for p*TERT* were performed to search for DNA mutations, but there were no significant differences identified between the nuclear grades. The exact searches were performed for primary and metastatic or recurrent lesions as well as for good- and poor-prognosis groups, but no repeatable mutations were detected. We, therefore, considered it unlikely that somatic mutations were involved in the change in nuclear morphology and malignant transformation in MLS.

Subsequently, we evaluated the mRNA expression in a comprehensive manner. The heatmaps of the gene expression profiles were drawn, and samples were clustered into groups that proved to be consistent with the ones determined by the modified Fuhrman grading. This finding suggests that the nuclear morphology evaluation method validates the gene expression behavior. We then performed GO and Reactome pathway analyses, and the results showed that the expression of cell cycle–related genes was significantly upregulated in the high–nuclear-grade group. Furthermore, we focused on three genes (namely, *FOXM1*, *PLK1*, and *CDK1*) identified from the PPI network and topology analysis after considering the fold change and statistical significance of DEGs, and after consulting the findings of previous studies.[36–38]

Finally, immunohistochemical staining was performed to verify the correlation between the mRNA and protein expression of the DEGs. The expression of all proteins was significantly increased in the high–nuclear-grade group and survival analyses revealed that the group of samples with both a FOXM1 and a CDK1 positivity had a significantly poorer DFS than those with other combinations. We, therefore, hypothesize that the increased expression of hub genes such as *FOXM1* and *CDK1* may positively regulate the expression of other cell cycle–related genes and result in poor prognosis in high–nuclear-grade MLS cases.

FOXM1, PLK1, and CDK1 are all well-known cell cycle–related factors. They act as proto-oncogenes in several cancer types and have been reported as poor prognostic factors.[38–42] PLK1 can lead to inappropriate chromosome segregation, aneuploidy, and tumorigenesis.[43] CDK1 makes the cell cycle shift from the G2 to the M phase.[44] FOXM1 plays a vital role in cell cycle progression and regulates the expression of many G2/M-specific genes that is essential for maintaining the chromosome segregation and genomic stability.[45,46] Both CDK1 and PLK1 act in the direction of promoting FOXM1.[38] Thus, they are strongly interrelated, and ultimately converge in cell cycle promotion. Regarding the mechanism for causing nuclear atypia, genes that may affect nuclear morphology were not identified in the present study. Although it was suggested that sporadic cases with the unique histological phenotype of a modified Fuhrman grade 4 might show unique gene expression profiles, additional studies with multiple cases are required to confirm this assumption.

This study has some limitations. The samples had deteriorated, leading to poor genetic examination, resulting in fewer cases, a shorter follow-up period, and fewer death or relapse events. Hence, the statistical power might be insufficient, and multivariable analysis could not be performed. The cellularity may not have been a significant poor prognostic factor in this study due to the low statistical power. It is worth noting, however, that nuclear gradings were found to be prognostic factors under the same circumstances.

In conclusion, our analyses suggest that an evaluation focusing on nuclear morphology (rather than cellular density) is more helpful in predicting MLS prognosis. This implication was emphasized by the differences in objective parameter measurements and revealed gene expression profiles. In addition, the modified Fuhrman grading can efficiently evaluate the nuclear atypia of the MLS cases.

ACKNOWLEDGMENTS

The authors would like to thank Enago (www.enago.com) for the English language review.

FUNDING INFORMATION

This work was supported by JSPS KAKENHI (grant number: 19H03444, 21K06887, and 21K20805).

CONFLICT OF INTEREST

Yoshinao Oda is an editorial board member of *Cancer Science*. The other authors have no conflicts of interest.

ETHICS STATEMENT

Approval of the research protocol by an Institutional Reviewer Board: the present study was approved by the Kyushu University Committee of Bioethics (approval no. 29–429 and 29–625).

Informed Consent: N/A.

Registry and the Registration No. of the study/trial: N/A.

Animal Studies: N/A.

ORCID

Yoshinao Oda https://orcid.org/0000-0001-9636-1182

REFERENCES

1. Fischer EG. Nuclear morphology and the biology of cancer cells. *Acta Cytol*. 2020;64:511-519.
2. Jevtic P, Levy DL. Mechanisms of nuclear size regulation in model systems and cancer. *Adv Exp Med Biol*. 2014;773:537-569.
3. Chow KH, Factor RE, Ullman KS. The nuclear envelope environment and its cancer connections. *Nat Rev Cancer*. 2012;12:196-209.
4. Rabjerg M, Gerke O, Engvad B, Marcussen N. Comparing World Health Organization/International Society of Urological Pathology Grading and Fuhrman Grading with the prognostic value of nuclear area in patients with renal cell carcinoma. *Uro*. 2021;1:2-13.
5. WHO Classification of Tumours Editorial Board. *Soft Tissue and Bone Tumours*. 5th ed. IARC Press; 2020.
6. Goldblum J, Weiss S, Folpe AL. *Enzinger and Weiss's Soft Tissue Tumors*. 7th ed. Elsevier; 2019.
7. Penel N, Coindre JM, Giraud A, et al. Presentation and outcome of frequent and rare sarcoma histologic subtypes: a study of 10,262 patients with localized visceral/soft tissue sarcoma managed in reference centers. *Cancer*. 2018;124:1179-1187.
8. Hoffman A, Ghadimi MP, Demicco EG, et al. Localized and metastatic myxoid/round cell liposarcoma: clinical and molecular observations. *Cancer*. 2013;119:1868-1877.
9. Moreau LC, Turcotte R, Ferguson P, et al. Myxoid/round cell liposarcoma (MRCLS) revisited: an analysis of 418 primarily managed cases. *Ann Surg Oncol*. 2012;19:1081-1088.
10. Haniball J, Sumathi VP, Kindblom LG, et al. Prognostic factors and metastatic patterns in primary myxoid/round-cell liposarcoma. *Sarcoma*. 2011;2011:538085.
11. Kilpatrick SE, Doyon J, Choong PFM, Sim FH, Nascimento AG. The clinicopathologic spectrum of myxoid and round cell liposarcoma: a study of 95 cases. *Cancer*. 1996;77:1450-1458.
12. Nezu Y, Hagiwara K, Yamamoto Y, et al. miR-135b, a key regulator of malignancy, is linked to poor prognosis in human myxoid liposarcoma. *Oncogene*. 2016;35:6177-6188.
13. ten Heuvel SE, Hoekstra HJ, van Ginkel RJ, Bastiaannet E, Suurmeijer AJ. Clinicopathologic prognostic factors in myxoid liposarcoma: a retrospective study of 49 patients with long-term follow-up. *Ann Surg Oncol*. 2007;14:222-229.
14. Kunieda J, Yamashita K, Togashi Y, et al. High prevalence of TERT aberrations in myxoid liposarcoma: TERT reactivation may play a crucial role in tumorigenesis. *Cancer Sci*. 2022;113:1078-1089.
15. Fiore M, Grosso F, Lo Vullo S, et al. Myxoid/round cell and pleomorphic liposarcomas: prognostic factors and survival in a series of patients treated at a single institution. *Cancer*. 2007;109:2522-2531.
16. Oda Y, Yamamoto H, Takahira T, et al. Frequent alteration of p16(INK4a)/p14(ARF) and p53 pathways in the round cell component of myxoid/round cell liposarcoma: p53 gene alterations and reduced p14(ARF) expression both correlate with poor prognosis. *J Pathol*. 2005;207:410-421.
17. WHO Classification of Tumours Editorial Board. *Urinary and Male Genital Tumours*. 5th ed. IARC Press; 2022.
18. Fuhrman SA, Lasky LC, Limas C. Prognostic significance of morphologic parameters in renal cell carcinoma. *Am J Surg Pathol*. 1982;6:655-663.
19. Kundel HL, Polansky M. Measurement of observer agreement. *Radiology*. 2003;228:303-308.
20. McHugh ML. Interrater reliability: the kappa statistic. *Biochem Med (Zagreb)*. 2012;22:276-282.
21. Kuwayama R, Suzuki K, Nakamura J, et al. Establishment of mouse model of inherited PIGO deficiency and therapeutic potential of AAV-based gene therapy. *Nat Commun*. 2022;13:3107.
22. Bankhead P, Loughrey MB, Fernandez JA, et al. QuPath: open source software for digital pathology image analysis. *Sci Rep*. 2017;7:16878.
23. Ishihara S, Yamamoto H, Iwasaki T, et al. Histological and immunohistochemical features and genetic alterations in the malignant progression of giant cell tumor of bone: a possible association with TP53 mutation and loss of H3K27 trimethylation. *Mod Pathol*. 2021;35:640-648.
24. Iura K, Kohashi K, Hotokebuchi Y, et al. Cancer-testis antigens PRAME and NY-ESO-1 correlate with tumour grade and poor prognosis in myxoid liposarcoma. *J Pathol Clin Res*. 2015;1:144-159.
25. Robinson MD, McCarthy DJ, Smyth GK. edgeR: a Bioconductor package for differential expression analysis of digital gene expression data. *Bioinformatics*. 2010;26:139-140.
26. Ashburner M, Ball CA, Blake JA, et al. Gene ontology: tool for the unification of biology. *Nat Genet*. 2000;25:25-29.
27. Yu G, He QY. ReactomePA: an R/Bioconductor package for reactome pathway analysis and visualization. *Mol Biosyst*. 2016;12:477-479.
28. Szklarczyk D, Morris JH, Cook H, et al. The STRING database in 2017: quality-controlled protein-protein association networks, made broadly accessible. *Nucleic Acids Res*. 2017;45:D362-D368.
29. Doncheva NT, Assenov Y, Domingues FS, Albrecht M. Topological analysis and interactive visualization of biological networks and protein structures. *Nat Protoc*. 2012;7:670-685.
30. Meyerholz DK, Beck AP. Principles and approaches for reproducible scoring of tissue stains in research. *Lab Invest*. 2018;98:844-855.
31. Kraus JA, Dabbs DJ, Beriwal S, Bhargava R. Semi-quantitative immunohistochemical assay versus oncotype DX® qRT-PCR assay for estrogen and progesterone receptors: an independent quality assurance study. *Mod Pathol*. 2012;25:869-876.

32. Heagerty PJ, Lumley T, Pepe MS. Time-dependent ROC curves for censored survival data and a diagnostic marker. *Biometrics*. 2000;56(2):337-344.
33. Ferreira MSV, Crysandt M, Braunschweig T, et al. Presence of TERT promoter mutations is a secondary event and associates with elongated telomere length in myxoid liposarcomas. *Int J Mol Sci*. 2018;19:608.
34. Koelsche C, Renner M, Brandt WHR, et al. TERT promoter hotspot mutations are recurrent in myxoid liposarcomas but rare in other soft tissue sarcoma entities. *J Exp Clin Cancer Res*. 2014;33:33.
35. Demicco EG, Torres KE, Ghadimi MP, et al. Involvement of the PI3K/Akt pathway in myxoid/round cell liposarcoma. *Mod Pathol*. 2012;25:212-221.
36. Trautmann M, Cheng YY, Jensen P, et al. Requirement for YAP1 signaling in myxoid liposarcoma. *EMBO mol Med*. 2019;11:e9889.
37. Isfort I, Elges S, Cyra M, et al. Prevalence of the hippo effectors YAP1/TAZ in tumors of soft tissue and bone. *Sci Rep*. 2019;9:19704.
38. Liao GB, Li XZ, Zeng S, et al. Regulation of the master regulator FOXM1 in cancer. *Cell Commun Signal*. 2018;16:57.
39. Dibb M, Han N, Choudhury J, et al. The FOXM1-PLK1 axis is commonly upregulated in oesophageal adenocarcinoma. *Br J Cancer*. 2012;107:1766-1775.
40. Yang W, Cho H, Shin H-Y, et al. Accumulation of cytoplasmic Cdk1 is associated with cancer growth and survival rate in epithelial ovarian cancer. *Oncotarget*. 2016;7:49481-49497.
41. Kuda M, Kohashi K, Yamada Y, et al. FOXM1 expression in rhabdomyosarcoma: a novel prognostic factor and therapeutic target. *Tumour Biol*. 2016;37:5213-5223.
42. Shibui Y, Kohashi K, Tamaki A, et al. The forkhead box M1 (FOXM1) expression and antitumor effect of FOXM1 inhibition in malignant rhabdoid tumor. *J Cancer Res Clin Oncol*. 2021;147:1499-1518.
43. Lee KS, Oh DY, Kang YH, Park JE. Self-regulated mechanism of Plk1 localization to kinetochores: lessons from the Plk1-PBIP1 interaction. *Cell Div*. 2008;3:4.
44. Enserink JM, Kolodner RD. An overview of Cdk1-controlled targets and processes. *Cell Div*. 2010;5:11.
45. Wierstra I, Alves J. FOXM1, a typical proliferation-associated transcription factor. *Biol Chem*. 2007;388:1257-1274.
46. Laoukili J, Kooistra MR, Bras A, et al. FoxM1 is required for execution of the mitotic programme and chromosome stability. *Nat Cell Biol*. 2005;7:126-136.

SUPPORTING INFORMATION

Additional supporting information can be found online in the Supporting Information section at the end of this article.

How to cite this article: Kawaguchi K, Kohashi K, Iwasaki T, et al. Prognostic value of nuclear morphometry in myxoid liposarcoma. *Cancer Sci*. 2023;114:2178-2188. doi:10.1111/cas.15729